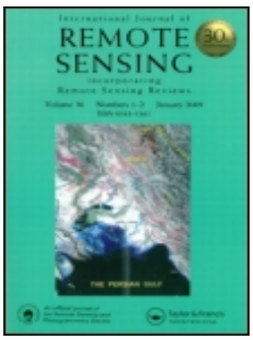

International Journal of Remote Sensing

ISSN: 0143-1161 (Print) 1366-5901 (Online) Journal homepage: http://www.tandfonline.com/loi/tres20

Change detection of buildings from satellite imagery and lidar data

José A. Malpica , María C. Alonso , Francisco Papí , Antonio Arozarena & Alex Martínez De Agirre

To cite this article: José A. Malpica , María C. Alonso , Francisco Papí , Antonio Arozarena & Alex Martínez De Agirre (2013) Change detection of buildings from satellite imagery and lidar data, International Journal of Remote Sensing, 34:5, 1652-1675, DOI: 10.1080/01431161.2012.725483

To link to this article: https://doi.org/10.1080/01431161.2012.725483

International Journal of Remote Sensing
Vol. 34, No. 5, 10 March 2013, 1652–1675

Taylor & Francis
Taylor & Francis Group

Change detection of buildings from satellite imagery and lidar data

José A. Malpica[a]*, María C. Alonso[a], Francisco Papí[b], Antonio Arozarena[b], and Alex Martínez De Agirre[a]

[a]*Mathematics Department, Alcalá University, 28871 Madrid, Spain;* [b]*Remote Sensing Department, National Geographic Institute, 28003 Madrid, Spain*

(*Received 30 June 2010; accepted 6 March 2012*)

Geospatial objects change over time and this necessitates periodic updating of the cartography that represents them. Currently, this updating is done manually, by interpreting aerial photographs, but this is an expensive and time-consuming process. While several kinds of geospatial objects are recognized, this article focuses on buildings. Specifically, we propose a novel automatic approach for detecting buildings that uses satellite imagery and laser scanner data as a tool for updating buildings for a vector geospatial database. We apply the support vector machine (SVM) classification algorithm to a joint satellite and laser data set for the extraction of buildings. SVM training is automatically carried out from the vector geospatial database. For visualization purposes, the changes are presented using a variation of the traffic-light map. The different colours assist human operators in performing the final cartographic updating. Most of the important changes were detected by the proposed method. The method not only detects changes, but also identifies inaccuracies in the cartography of the vector database. Small houses and low buildings surrounded by high trees present significant problems with regard to automatic detection compared to large houses and taller buildings. In addition to visual evaluation, this study was checked for completeness and correctness using numerical evaluation and receiver operating characteristic curves. The high values obtained for these parameters confirmed the efficacy of the method.

1. Introduction

Although a wide range of modern geographical products are available, cartography remains an important task for today's national mapping agencies (NMAs). User demands have increased and diversified and this has placed increased pressure on NMAs to operate more efficiently and effectively. The NMAs are now expected to generate more and better products and services in less time. This includes the production of topographic databases for territories, which is one of the primary priority tasks of NMAs. The creation, maintenance, and production of high-quality topographic databases all require software that understands the craft of the cartographer for application to an automated production environment.

In recent years, most NMAs in developing countries have implemented basic cartographic digital databases. They are now developing derived products on several scales, but the current problem is the maintenance of these topographic databases. Considerable effort is being expended to find efficient software for this enterprise, especially for the mapping of urban areas, which require frequent updating. Today, this updating is carried

*Corresponding author. Email: josea.malpica@uah.es

ISSN 0143-1161 print/ISSN 1366-5901 online

http://dx.doi.org/10.1080/01431161.2012.725483
http://www.tandfonline.com

(*a*) (*b*) (*c*)

Figure 1. (*a*) Demolished buildings; (*b*) new buildings; and (*c*) planimetric inaccuracies.

out manually by visual inspection of orthophotos to detect changes in cartographic entities – a task that is both time consuming and expensive. Therefore, the establishment of semi-automatic procedures would be of great benefit as these could significantly reduce map revision timelines. The Spanish NMA has recently completed its national topographic database at the scale of 1:25,000, but this database already needs to be updated. The present study has concentrated exclusively on buildings in this database, with the objective of detection of the changes in this entity type between two specific dates.

Change detection involves the study of a pair of images taken from the same geographical area, but acquired at different times, in order to detect the changes that have occurred between the dates of the two data collections. In our work, instead of comparing pairs of images, we have compared an old map, constructed using digital cartographic procedures as vector data, with more recent spatial information of the same geographical area acquired from satellite images (raster) and laser data. Detecting these changes in this way allows for the possibility of automatically updating the maps.

In the present study, the results of the changes are depicted in a modification of the well-known traffic-light detection map, where the different types of change are represented by different colours. Ultimately, a human operator would perform future updates aided by the colours of the traffic-light detection map. The proposed procedure can detect several types of changes in the following categories: (1) demolished buildings; (2) new buildings; and (3) planimetric inaccuracies. As noted in Figure 1(*a*), some of the buildings in the digital cartography represented by the red lines have been demolished in recent years. This would indicate that these buildings need to be removed from the vector database as part of the updating process. As noted in Figure 1(*b*), several new buildings are seen that do not appear in the digital cartography. These newly constructed buildings would therefore need to be included in an updated vector database. As noted in Figure 1(*c*), planimetric inaccuracy can be observed in the digital orthophoto, where a displacement is evident in the base of the buildings with respect to the vector cartography. This information would also need to be corrected in the updated database.

2. State of the art

Many methods and techniques for change detection have been published in the last three decades; reviews can be found in Lu et al. (2003) and Coppin et al. (2004). Given the importance of space imagery as a source for updating maps, several working groups have been

created over the past few years and several workshops have been organized on the topic of updating maps using high-resolution data. Many map entities, such as roads (Mena and Malpica 2005; Mancini, Frontoni, and Zingaretti 2010), vegetation (Hayes and Sader 2001), land cover (Marcal et al. 2005), etc., can be updated. The present article deals specifically with buildings.

The pioneering work on the detection of buildings for automated map updating can be traced to project ATOMI (Automated Reconstruction of Topographic Objects from Aerial Images using Vectorized Map Information), a cooperative venture between the Swiss Federal Office of Topography and the Institute of Geodesy and Photogrammetry at ETH Zürich. This project used a vectorial database (VECTOR25) at scale 1:25,000, and exploited Niederöst's assessment (Niederöst 2003) that VECTOR25 favours the detection of buildings. One aim of the present project was to develop a software prototype for a productive system. Several procedures were analysed: one of these combined height information and three-dimensional (3D) edges. The method subsequently used by Olsen (2004) for the detection of change was realized in three phases: (1) extraction of the cartographic entities that are used as training samples; (2) identification of the buildings by means of a supervised and unsupervised classification; and (3) elaboration of a map of the traffic-light type of changes, where a final editing must be completed by a human operator.

The problem with Olsen's method was that it did not detect buildings that were different from the buildings used as training samples for the algorithm. In later work (Olsen and Knudsen 2005, 2006), the authors realized the importance of height with regard to detecting buildings and they indicated the necessity of using the digital surface model (DSM), which is calculated using stereoscopic pairs. Knudsen and Nielsen (2004) employed other characteristics (spectral, texture, and shape), but again, reliable results were not obtained unless the heights were also considered. For this reason, these authors proposed to investigate new characteristics, such as shadows, since shadows are another method of introducing height. Peng and Liu (2005) also found that consideration of shadows led to satisfactory performance. Nakagawa and Shibasaki (2008) also introduced the concept of shadows fused with textures and achieved acceptable results.

Matikainen, Hyyppä, and Hyyppä (2003) and Matikainen, Hyyppä, and Kaartinen (2004) reported that, in general, experiments incorporating light detection and ranging (lidar) or precision DSM produced better results. More recently, these authors have applied decision trees for this type of analysis (Matikainen, Kaartinen, and Hyyppä 2007). Vosselman, Gorte, and Sithole (2004) were able to use lidar and two classifications to separate vegetation, building types, and trees and shrubs. Huang and Chen (2007) investigated the fusion of lidar and aerial images, comparing images from 2002 with images from 2005. The images from 2002 and 2005 also contained lidar information and the authors were able to obtain good results using mathematical morphology. Alonso and Malpica (2008) studied the influence of lidar on the classification of multispectral Système Pour l'Observation de la Terre 5 (SPOT5) imagery over a semi-urban area and obtained an improvement of 28.3% when lidar was included. Chen et al. (2009) used lidar and QuickBird images to extract buildings and highways, using a hierarchical method of object orientation, and obtained overall accuracies of 89%.

All of these studies emphasize height as a fundamental measurement for detecting buildings. For this reason, we have introduced lidar as a complement to SPOT imagery. Recently, Liu et al. (2010) developed a semi-automatic method for detecting changes in urban buildings using UltraCamD images and an existing 3D computer-aided design (CAD) map. The purpose of the present study is to detect changes that occur after natural

disasters such as earthquakes, typhoons, or tsunamis. Most of the change detection methods proposed above, as well as our own, could serve this purpose.

The EuroSDR is the European organization that links NMAs, research institutes, and universities that are active in applied research in geographical spatial data. It periodically issues projects to debate and to compare the leading techniques in cartography and photogrammetry being investigated in the academic and professional fields. The intent of these projects is to discover the productive viability of the theoretical methods. In 2005, EuroSDR introduced a new project with the following objectives: (1) to evaluate the possibility of automatically detecting changes in constructions in cadastral databases; (2) to observe the benefits when specific data are introduced (e.g. lidar/DSM/infrared images); (3) to analyse the value of certain developments, such as comparing the methods that use the cadastral database to obtain the final solution with the methods that use only images; and (4) to study the best scale for comparison of data in the process of change detection. The results and findings from the EuroSDR groups are summarized by Champion, Stamon, and Pierrot-Deseilligny (2009b).

Our present work shares these objectives and our comparison between algorithms is based on the protocol established by EuroSDR. Although we used our own imagery and data, we manually evaluated our method with a reference database by calculating the number of true positives (buildings in the cartographic database reported as demolished or new (i.e. changed) that are actually changed in the reference), false positives (buildings that have not changed in the reference, but were reported as changed by the method), and false negatives (buildings that had changed in the reference, but were reported as unchanged) to test the method's suitability (i.e. to evaluate the completeness and correctness of the method). The quality measures are computed in the evaluation on a per-building basis, instead of on a per-pixel basis, as recommended by EuroSDR. This is probably the most meaningful way of presenting these types of results, as observed in the 2009 EuroSDR Report (p. 56), which stated 'a change detection approach is limited by the number of changed buildings that is missed or over-detected, and not by the area covered by these buildings'.

3. Study area and data

3.1. Satellite data

Several authors have utilized imagery from satellites for detection and extraction of buildings. For example, Mayunga, Coleman, and Zhang (2007) used QuickBird and Lhomme et al. (2009) used IKONOS and QuickBird. The present study used images from SPOT5, which was launched on 4 May 2002. The data are generated as four multispectral bands and a panchromatic band, as follows: green B1 0.50–0.59 μm; red B2 0.61–0.68 μm; near infrared B3 0.78–0.89 μm; infrared B4 1.58–1.75 μm; and panchromatic 0.50–0.73 μm. The first three bands have a spatial resolution of 10 m, the fourth band has a spatial resolution of 20 m, and the panchromatic band has a spatial resolution of 2.5 m. Images were taken from an altitude of 822 km, with a digitalization of one byte per pixel. The dimensions of the complete scene were 60 km × 60 km. The image used in our present work (Figure 2) corresponds to a site approximately 6 km × 6 km located in Alcalá de Henares, about 30 km east of the city of Madrid. The Henares River crosses the study area from east to west. The university campus area, consisting primarily of university buildings, is situated in the upper part of the study area. As Figure 2 demonstrates, the image depicts thousands

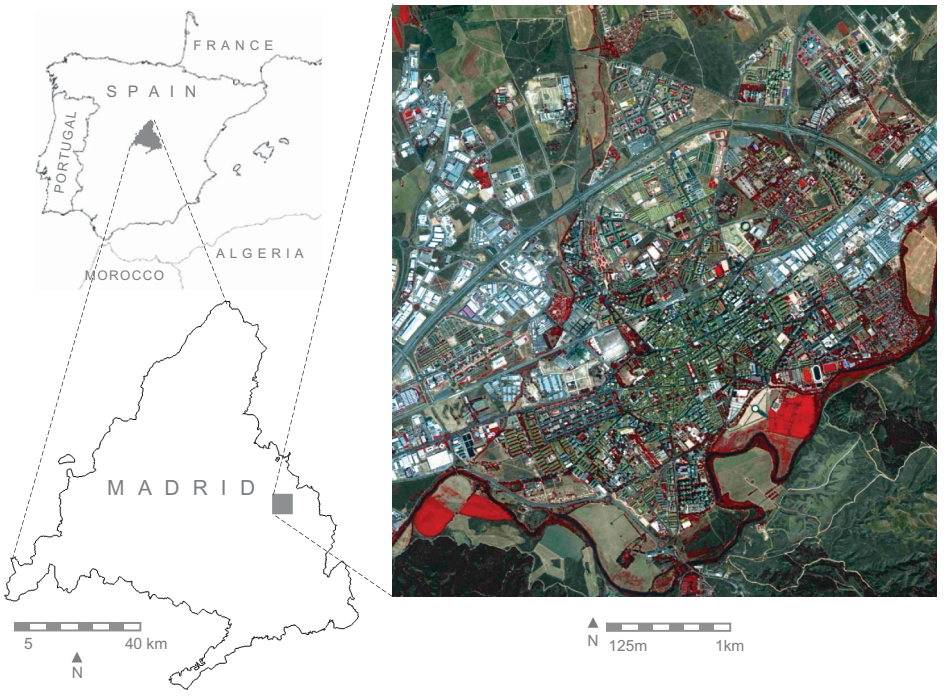

Figure 2. Pan-sharpened SPOT5 image of the study area. This depicts a false colour image composition of bands B1, B2, and B3 as RGB.

of buildings of varying types and forms. The terrain is relatively flat, but the riverside area to the left, in the southern part of the image, is hilly, with altitude differences of 200 m.

Using the four multispectral and the panchromatic images, we applied the principal component analysis (PCA) pan-sharpening method (Figure 2). We chose the PCA method from among several methods that could have been applied (Wald 2002) because, together with Brovery transforms and intensity–hue–saturation, it provides superior visual high-resolution multispectral images, although it disregards the requirement for high-quality synthesis of spectral information (Wang, Ziou, and Armenakis 2005). One important advantage of PCA is that it is rapid, and since the final objective is an interactive software application to help human operators perform map updating, a compromise between speed and image quality has been sought.

Precise georeferencing was necessary because the image has to be superimposed on the lidar data and the vector cartography. Errors of less than one pixel were obtained, which means a dimension of less than 2.5 m. The georeferencing of the image was supported via the metadata for SPOT5, and 20 points were surveyed in the field using the global positioning system (GPS) with sub-centimetre accuracy and manually measured on the image. Overall, nine ground control points (GCPs) were sufficient for compensation for systematic errors inherent in the model and to obtain sub-pixel accuracy. The remaining 11 points were used as independent checkpoints. The calculation was performed with the help of PCI software, specifically using the rigorous sensor model for pushbroom linear array sensors (Toutin 2004). This method has a high modelling accuracy (approximately

one pixel or better) and great robustness (Malpica, Mena, and Gonzalez-Matesanz 2007), and uses only a few GCPs to achieve consistent results over the full image.

The raster layer for the lidar arises, as an interpolation, from the cloud of points of the lidar file, which has its own georeferencing from the GPS sensor on board the aeroplane. The lidar layer was co-registered to the SPOT image using well-known tie points in the SPOT5 image layer and the lidar layer. The vectorial data from the Base Cartográfica Nacional (BCN) were used with their original coordinate from the cartographic database, without any co-registering. When no correspondence existed between the map and the image, the error was assumed to come from the map, since that layer was produced manually. These cartographic human errors are shown by the algorithm, as indicated in Section 5.

3.2. Lidar

Lidar technology allows the calculation of the DSM with a precision of the order of 20 cm in planimetry and 30 cm in height (Raber et al. 2002). The combination of a sweeping beam laser with inertial navigation systems and a GPS guarantees a high geometric precision in the data. In this study, we used the LEICA ALS50-II (Leica Geosystems AG, Heerbrugg, Switzerland) sensor to capture the lidar data.

Although a DSM could also be obtained by classical digital photogrammetry, this would be more expensive and slower to produce. The lidar data used in the present work correspond to two successive flights, conducted in the mornings of 17 and 19 May 2006. The flight was taken at an altitude of approximately 1800 m. We obtained 144 blocks of 1 km^2 each. Of these, we selected 33 blocks that agreed geographically with the other data (SPOT5 and vector cartography) available for our work. All data selection was carried out with the intention of including the entire city of Alcalá de Henares. The point density of the lidar data was 0.5 point per square metre, which meant about three points for each SPOT5 pixel. The coordinate system is WGS84 with orthometric heights.

The DSM was obtained from the first echo of each pulse, after filtering the noise that was generated in the process of data capture. We rasterized the 3D clouds of the LAS file using the method proposed by Streutker and Glenn (2006), who divided the data into regular cells, with each cell containing a determinate number of individual lidar points, depending on the local density of each cell. The final elevation for each cell was calculated as the average of several lidar points contained within that cell: if a cell was without points, then a nearest neighbour interpolation was applied. The dimension of the cells (i.e. the resolution) was 1 m. The DSM contained information regarding constructions, vegetation, and uncultivated ground, as seen in Figure 3(*a*). The digital terrain model (DTM) was generated as a product derived from the DSM after employing a semi-automatic method developed recently by Martinez de Agirre and Malpica (2010). This method consists of applying several filters to the DSM, with the intention of removing the non-ground points. Next, minimal manual editing of the points that had not been properly classified was necessary. Currently, no fully automatic method is available for obtaining a DTM from the DSM. The result is illustrated in Figure 3(*b*). Finally, calculation of the difference between the DSM and the DTM generated the standard DSM (nDSM) shown in Figure 3(*c*).

Initially, the lidar data come in a binary format (*.LAS), according to the ASPRS norm. The LAS format includes information in addition to echoes of the pulses, such as GPS time and intensity. If the first echo is considered, the image that appears in Figure 3(*d*) is obtained, while Figure 3(*e*) illustrates the image of the last echo. This latter layer is obtained with the same technique used for the first echo, as explained above. Figure 3(*f*) illustrates the difference between the images of the first and the last echoes. In this last

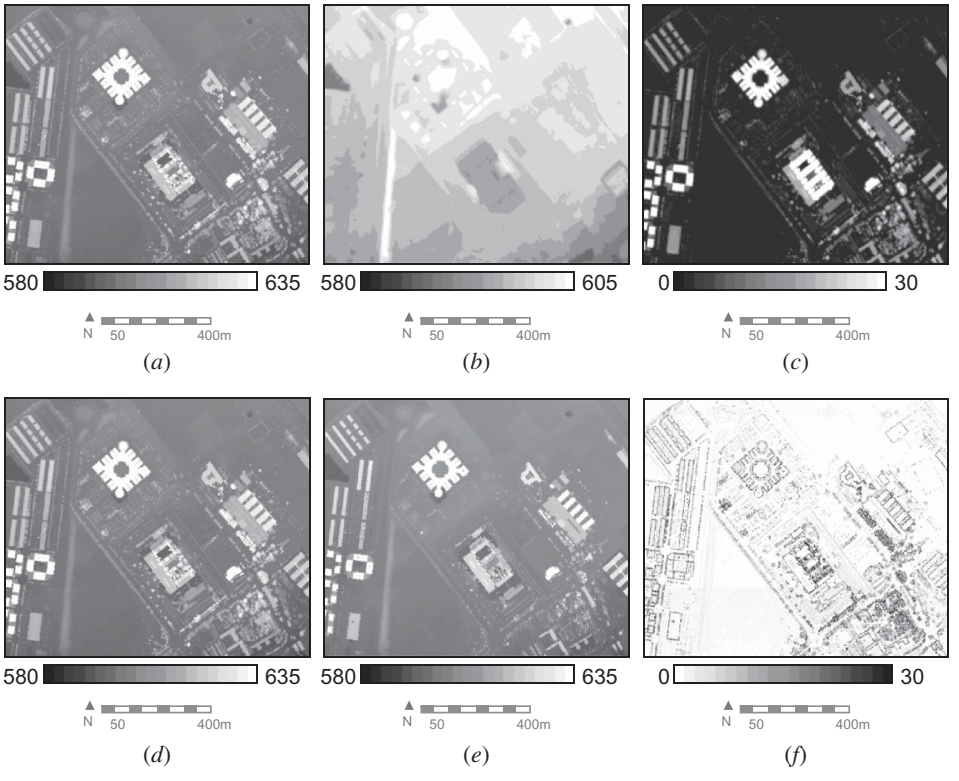

Figure 3. (*a*) DSM; (*b*) DTM; (*c*) nDSM; (*d*) first echo; (*e*) last echo; and (*f*) difference between echoes. Units are in metres.

image, which shows the case for the difference in echoes, darker pixels represent higher values than brighter pixels, i.e. the opposite of the other cases (Figures 3(*a*)–(*e*)).

In developing the method proposed in the present study, we found that working with the differences between these echoes proved very useful, as discussed in the next section. The differences between these echoes allowed us to differentiate between different types of vegetation, since a pulse can be reflected by leaves or by the ground.

The complete nDSM used with the algorithm developed in our work is shown in Figure 4.

3.3. Numerical cartographic database

In 1986, the Spanish NMA began the process of numerical production of a national topographic map at the scale of 1:25,000. Over the past two decades, the NMA has published 1:25,000 sheets for Spain's entire national territory and, at the same time, a DTM of 25 m grid and a numerical cartographic base called BCN at a scale of 1:25,000, which also captures information on the national territory. From this BCN, we can extract vector files for buildings. Figure 5 shows examples of the vector cartography overlaid on aerial images with 0.5 m resolution. These images were taken from the Spanish Mapping Agency PNOA (Arozarena and Villa 2005). Since the vector cartography has to represent the position of the buildings, the errors and geometric inaccuracies can be seen. Up to a certain point (5 m for 1:25,000 map scale), these errors are normal because vector cartography is a manual product and prone to human error.

Figure 4. nDSM (difference between DSM and DTM) of the city of Alcalá de Henares and its surroundings.

The BCN contains a great amount of information, with codes defined for each cartographic entity. All of the vector entities related to building construction must be extracted; these correspond to different codes depending on whether the building is residential, industrial, historical, etc. Each code is also associated with a colour and a width-of-line based on building type. Taking all of these codes into consideration, we applied several filters to the original BCN and obtained a vector layer for the buildings. Next, we generated a mask for buildings. For each of the building codes, the algorithm creates a region of interest (ROI) and creates a mask that joins all of these regions (an example can be seen in Section 4.2.3, Figure 8(*a*)).

4. Methods

4.1. Introduction

In our work, the integration of lidar with the multispectral images allowed for the discrimination of buildings and the implementation of an automatic system for the detection of changes. These sources of data combine the advantages of multispectral SPOT5 satellite

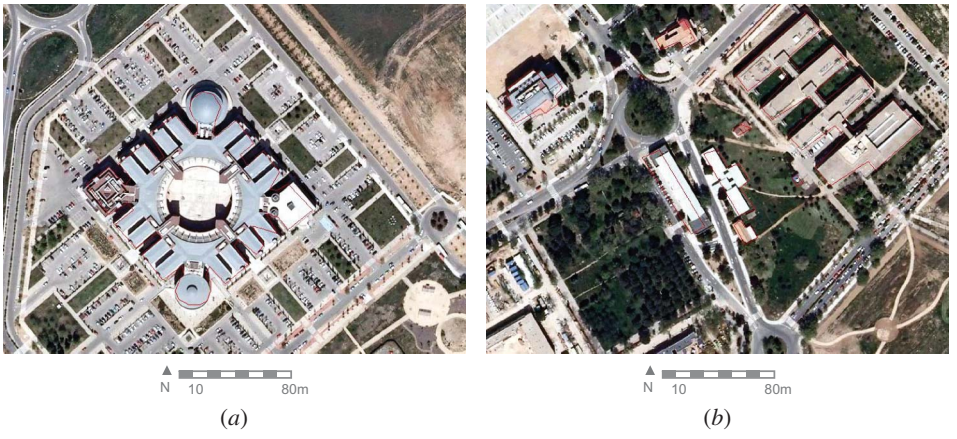

Figure 5. Vector cartography from the BCN in red (code 41) over aerial image with GSD 0.5 m. (*a*) Polytechnic School of Alcalá University and (*b*) different buildings from the university campus of Alcalá.

data with the height information provided by lidar. The input data consisted of SPOT5, lidar, and the digital vectorial cartography from the BCN, as can be observed in the upper part of the diagram (Figure 6). After pre-processing of these data, the support vector machine (SVM) was used for the central algorithms of this method. The ultimate objective was to obtain a map of changes.

4.2. SVM algorithm

Supervised learning implies analysis of the training set (which is a given set of labelled observations) in order to predict the labels of unlabelled future data. Specifically, the objective is to construct some function that describes the relationship between observations and their labels.

The SVM is a powerful technique for training binary classifiers from examples, and it seeks a hyperplane that will separate the labelled observations. Intuitively, a hyperplane that is as far away as possible from either class is preferable, because the results are expected to generalize better when applied to unseen future data. The idea of the SVM classifier appeared initially in a 1992 article by Boser, Guyon, and Vapnik (1992), where it was applied to a problem of recognition of characters. The authors demonstrated the superiority of the SVM against other algorithms for character recognition. Vapnik and the research team at AT&T laboratories developed different variants for the SVM algorithm (for more details, see Vapnik 1995).

SVMs are essentially binary classifiers by their inherent nature; however, they can be used to handle the multiple classification problems commonly needed in remote-sensing applications. The two approaches commonly used to accomplish this are the one-against-all and the one-against-one techniques. No superiority of one over the other has been reported so far (Hao, Liu, and Yang 2006).

The output of the SVM algorithm, when used as a binary classifier, is given by values between zero and one, similar to a probability layer. Formally speaking, these would be pseudo-probabilities. Since a pixel with a value close to one has a great probability of

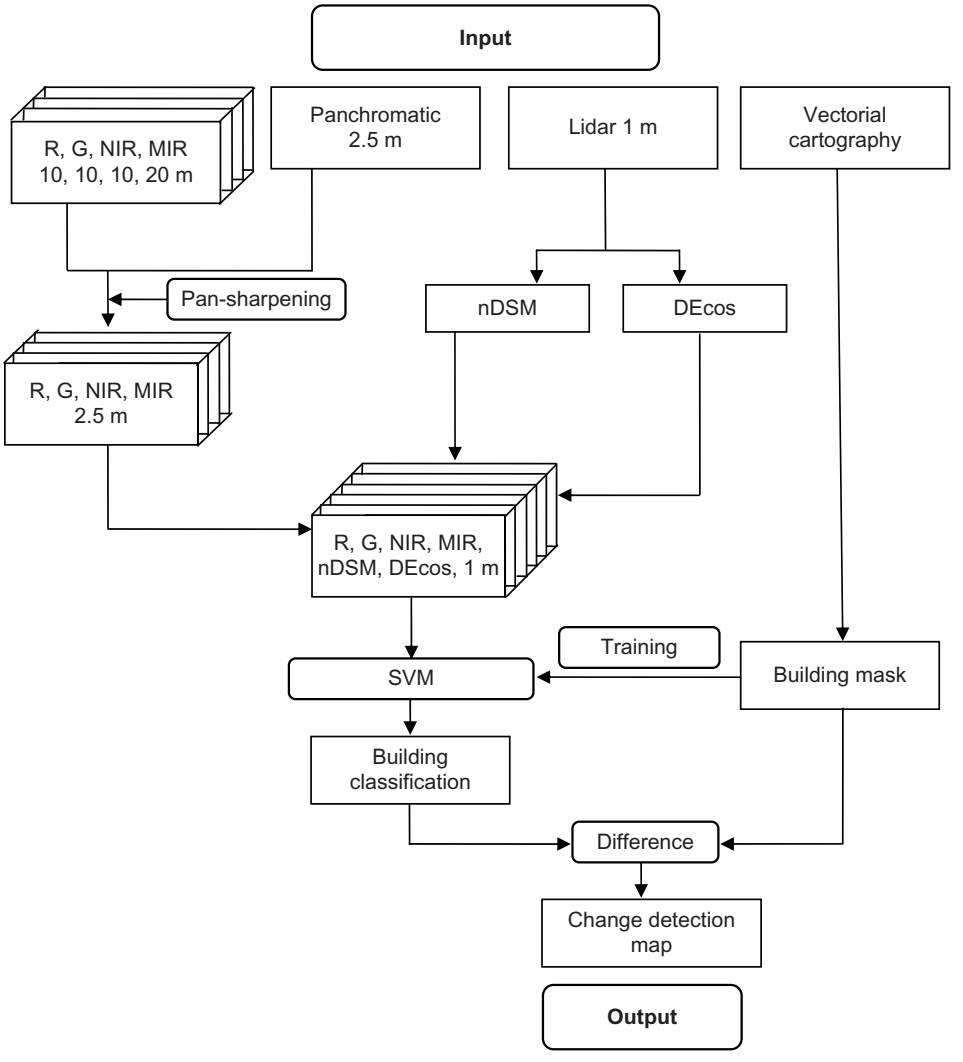

Figure 6. Flow diagram of the proposed algorithm. NIR, near infrared; MID, mid-infrared; R, red; G, green.

belonging to one class versus the other, we took these values as membership measures for our classification purposes.

4.2.1. Input to the SVM algorithm

The first input to the algorithm is given by

- the four bands of the SPOT5 image, with 2.5 m of spatial resolution, transformed with the pan-sharpening method;
- the normalized DTM, usually named nDSM, which represents the difference between the DSM and the DTM, as explained in Section 3.2; and

- the difference between the first and last echo of each pulse (DEcos), also explained in Section 3.2.

A file with the six bands was formed so that a pixel would be given by a vector with six components, all normalized to 0–255 levels of grey.

The other input to the algorithm is the vector layer from the BCN, as explained in Section 3.3. This vectorial layer is converted in a mask (building mask) necessary for the training, which will be explained in the next section. Ultimately, this mask is used to detect the changes by comparing the constructions obtained by the proposed algorithm (using SVM for classification) with the existing ones in the BCN vector layer. A flow chart that summarizes the proposed algorithm is shown in Figure 6.

4.2.2. Training

The following three classes have been considered: ground (ω_1), vegetation (ω_2), and buildings (ω_3). The training is automatically achieved by the algorithm from the vector layer. The proposed algorithm first generates a large number of random pixels for the whole image. For the case presented here (Figure 2), 5000 random points for each class were taken. From the experiments, we determined that taking a greater number of points makes no difference in the end result and just increases the time needed to execute the algorithm (this is 1 h, as will be explained in Section 4.2.5). The randomly generated pixels are assigned to a class as follows: if the randomly generated pixel meets certain conditions imposed for a class, it will be considered to belong to that specified class (see Figure 8). If these conditions are not met, the pixel is ruled out or disregarded. The parameters used to impose the conditions for each class are

h: height,
w_1: width of the window mask,
i: vegetation index,
w_2: width of the window difference of echoes, and
d: difference between echoes.

The units for these parameters are metres for h and d, number of pixels for w_1 and w_2, and dimensionless for i. After several experiments on different areas, the optimal values were determined to be $h = 2$, $w_1 = 5$, $i = 0.1$, $w_2 = 5$, and $d = 3$. These parameters were fixed for all of the subsequent tests. Small variations in the values did not affect the results, which showed the robust performance of the proposed method. The Buildings_M term, which indicates the mask of buildings (see Figures 7 and 8(a) for details of the building mask), was constructed from the files of the vector cartography of the buildings obtained from the BCN.

If a pixel belongs to the mask, it means that it corresponds to a zone where a building exists, according to the vector cartography. However, if the building has been demolished, further discrimination is needed with regard to the difference between echoes (Echoes_D) and the normalized difference vegetation index (NDVI), as can be seen in Figure 7.

4.2.3. Output from the SVM algorithm

After the classification of SVM, the layers of membership measure for each class are obtained. For application of the SVM, the radial basis kernel is used. The threshold for the new layer of membership measure of buildings becomes 0.5, and a new image (Figure 8(b))

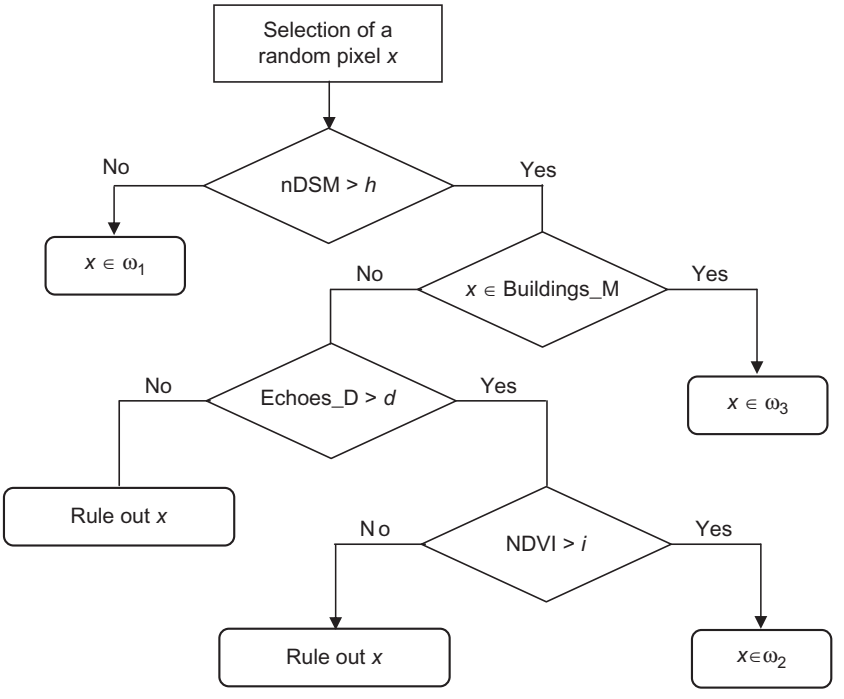

Figure 7. Flow diagram for selecting training samples.

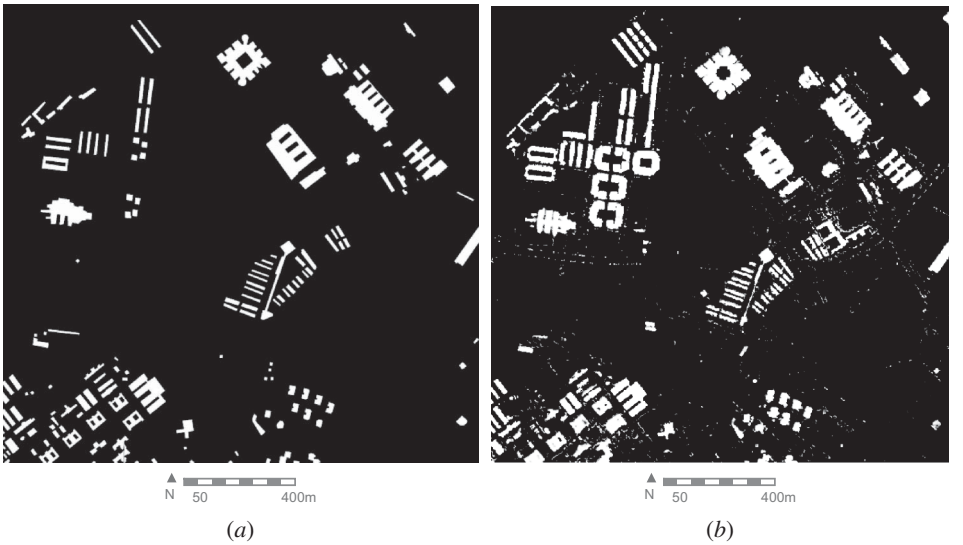

(*a*) (*b*)

Figure 8. (*a*) Mask for buildings from BCN and (*b*) output of the SVM algorithm.

of the buildings is obtained. Actually, the SVM algorithm discriminates between only two classes: vegetation and buildings (the building mask obtained from the vectorial data ignores ground pixels). Several values for this threshold were tried and no significant differences were observed in the output for values between 0.3 and 0.7. The robustness is very

high and the threshold can be taken as the middle value of the membership measure 0.5. The differences between Figures 8(*a*) and (*b*) are due to the detection of new buildings by the proposed algorithm using SVM for classification.

4.2.4. Change detection

In order to obtain the map of changes, the algorithm compares the mask of buildings obtained from the BCN (Figure 8(*a*)) with the new image of the buildings obtained from determining the layers of membership measure (Figure 8(*b*)), as discussed in the previous section.

4.2.5. Implementation

The algorithm is implemented in the IDL programming language as an extension of the ENVI software of Visual ITT Information Solutions (http://www.ittvis.com/). The large size of the images, vector data, and lidar preclude loading of everything into the computer RAM. Therefore, the input data are divided into smaller equal-sized (or near-equal) spatial units, the algorithm is run on these smaller pieces, and then the pieces are joined. As a result, the entire geographical area of Alcalá in Figure 2 was divided into a set of small rectangles or tiles. Algorithms were run on each tile and the tiles were finally joined. In ENVI, this is known as the tiling technique and it allows handling of images of any spatial size. The run-time on a PC (a 3 GHz CPU and 2 GB of RAM) is about 1 h for the size of the data shown in this study (36 km^2) (Figure 2). For a complete 1:25,000 map sheet, which is the standard for Spanish NMA (approximately 100 km^2), the run-time would be approximately 3 h.

5. Results

5.1. Types of change

The changes in this study were indicated using a variant of the traffic-light map technique, which has been well validated in the field of cartography (Heipke et al. 1997; Kraak and Ormeling 2003). When validating an algorithm that detects a certain cartographic entity, the traffic-light technique will consist of assigning the colour green for a correctly detected entity or building and it requires no further manual editing. The colour red will be assigned when the entity has been detected erroneously. The colour yellow will be assigned when the entity is partially erroneous. Since this study investigated more situations than usual, we have modified the general traffic-light technique. In our case, the following colours have been assigned to indicate different situations: new buildings are assigned the colour red, demolitions are assigned the colour blue, validations are assigned the colour green, incoherencies are assigned the colour yellow, and backgrounds are assigned the colour grey (see Figure 9).

5.2. Discussion

The final image of changes given by the proposed algorithm is shown in Figure 9. New residential and industrial areas of the city appear in red, as noted in the central part of the image, a little to the left. This represents an area called the *Garena*, which corresponds to a new construction zone developed as a result of a previous real estate boom in Spain. Figure 9 also shows another new construction zone, known as the *Extension*, in the upper

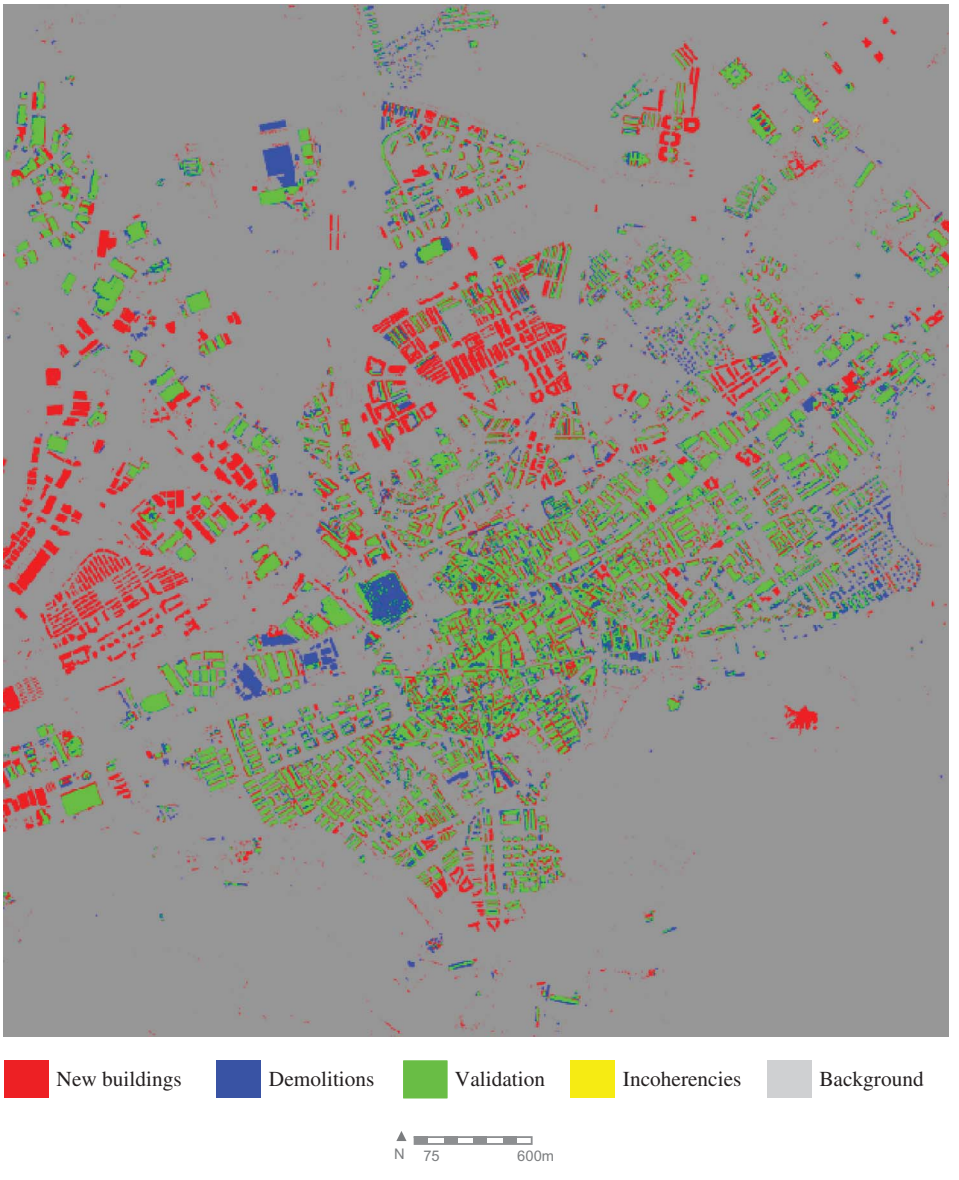

Figure 9. Change detection results for the entire study area (36.0 km^2).

central part of the image. In the old part of town, the green colour predominates, indicating that no significant changes have occurred in the time interval examined.

The efficiency of the method for the detection of buildings requires that the DTM, extracted from DSM lidar, be of high quality. Otherwise, the errors in the DTM will be seen as errors in the image changes that appear in the final results. As Figure 9 illustrates, the large red spot on the right side, a little below the middle of the image, corresponds to an error in the DTM. This spot indicates a small hill with steep sides that the algorithm (for forming the DTM from the DSM) mistook for a building and eliminated from the DSM

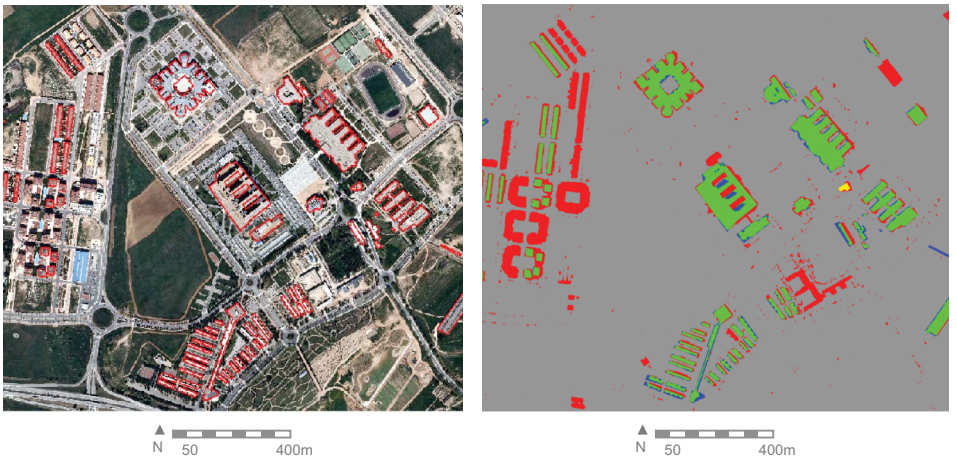

(*a*) (*b*)

Figure 10. (*a*) Aerial image with 0.5 m resolution for the university campus of Alcalá with vector cartography and (*b*) final results for (*a*).

when forming the DTM. The human operator in the later manual edition failed to spot this error and, thus, it was passed on to the DTM.

Figure 10 shows the oldest part of the campus of the University of Alcalá, including the polytechnic school, nursing school, medical school, and other buildings. The new buildings, appearing in red, were constructed after the creation of the vector cartography. All of these images were obtained directly from the proposed algorithm, and some noise can be observed; however, this noise could be eliminated with mathematical morphology by means of an opening operator. The yellow building (Figure 10(*b*)) represents an error in the original codification of the vector cartography; it has been registered with a code 11 when, in fact, it should have been registered with a code 41. Code 11 is reserved for inner patios, while code 41 is reserved for buildings. This type of incoherency arises because of the particular way the mask for buildings was made: the raster layer for code 11 (inner patios) was subtracted from the raster layer formed for code 41 (general buildings). If there is a mistake, and code 11 is written in place of code 41, then a –1 appears where only zeros or ones should appear if everything is correct in creating the mask for buildings. Therefore, if a –1 appears when the building mask is constructed, the incoherency is reported in yellow.

Figure 11 shows buildings that originally existed when the cartography was created, but were later demolished.

When the buildings are small, such as small isolated houses or huts, method detection problems can be identified, especially if vegetation exists around the house. Figure 12 shows that the uppermost hut is almost completely covered by a tree that has a height greater than that of the hut. In Figure 12(*e*), a false colour SPOT5 image has been placed, which has been pan-sharpened from multispectral images of 10 and 20 m, as described in Section 3.1. For this reason, the quality of the image is far lower when compared with the PNOA aerial image of 0.5 m resolution. It is important to remember that the image that drives the proposed algorithm is the SPOT5 (see the flow chart of the algorithm in Figure 6).

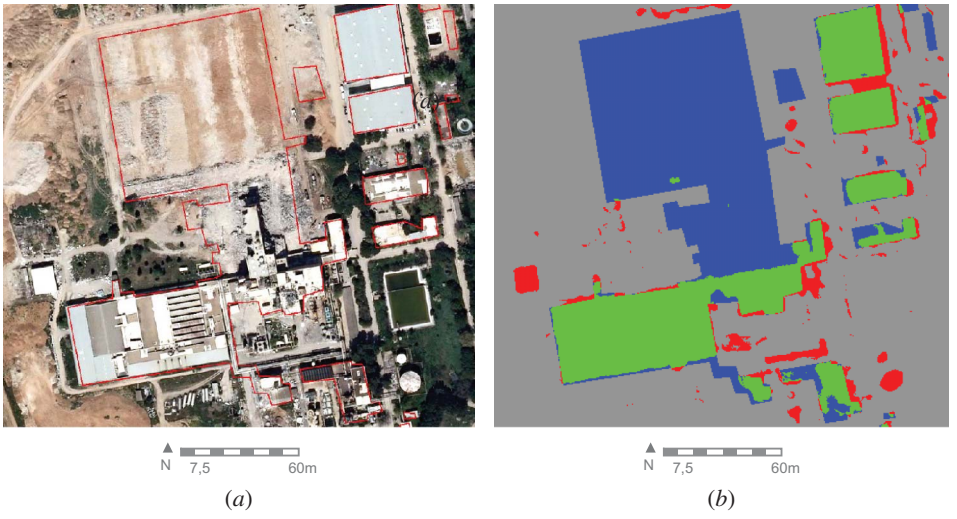

(*a*) (*b*)

Figure 11. Detection of a demolished building.

The aerial image of 0.5 m resolution was used for only visualization purposes. It was not used as an input to the proposed algorithm. The reason for not using aerial imagery is that the images that are available have only RGB values, while the SPOT5 images have two infrared bands, and infrared is very important for detecting vegetation. In the SPOT5 image, this hut is almost indistinguishable. The image is so poor that the hut could not be detected by the proposed algorithm. In the lidar image of the nDSM, the hut can only be seen as a small white spot that corresponds to a mixture of the vegetation and the hut. In these conditions, the proposed algorithm, by itself, has difficulty in detecting buildings of this size.

We also tried to input the PNOA aerial images instead of the SPOT5 imagery. A higher spatial resolution of the aerial image is obtained with PNOA than with the spectral high resolution available with the infrared bands of the SPOT5. After many experiments, the infrared bands proved to be more effective in separating vegetation and buildings than was the higher resolution aerial imagery. Figure 13 shows an example of an area in the centre of Alcalá city. Figure 13(*a*) represents the building mask from the vectorial cartographic BCN, while Figure 13(*b*) is the corresponding PNOA aerial image. Figure 13(*c*) is the result of applying the classification algorithm SVM to this area using only the PNOA aerial image, lidar data, and the vectorial cartography from the BCN. Figure 13(*d*) is the result of applying the SVM algorithm to the same area using SPOT5, lidar data, and the vectorial cartography. As can be observed in the centre of the image, some trees (Figure 13(*b*)) have been mistakenly confused with a new building (Figure 13(*c*), the approximately rectangular red figure), whereas it is not confused in Figure 13(*d*). With the aerial image, the algorithm could not discriminate vegetation from buildings, while it could with the SPOT5 imagery, and this is due to the two infrared bands. More groups of trees have been taken as new buildings in Figure 13(*c*), but this did not happen in Figure 13(*d*). The only new building in the area is well detected by both input data (aerial PNOA and SPOT5), but clearly more false positives are seen in the aerial image than in the SPOT5 image.

When the parameters for the aerial image input are changed, in order to reduce the false positives, old buildings are no longer detected, and new false negatives appear. In our

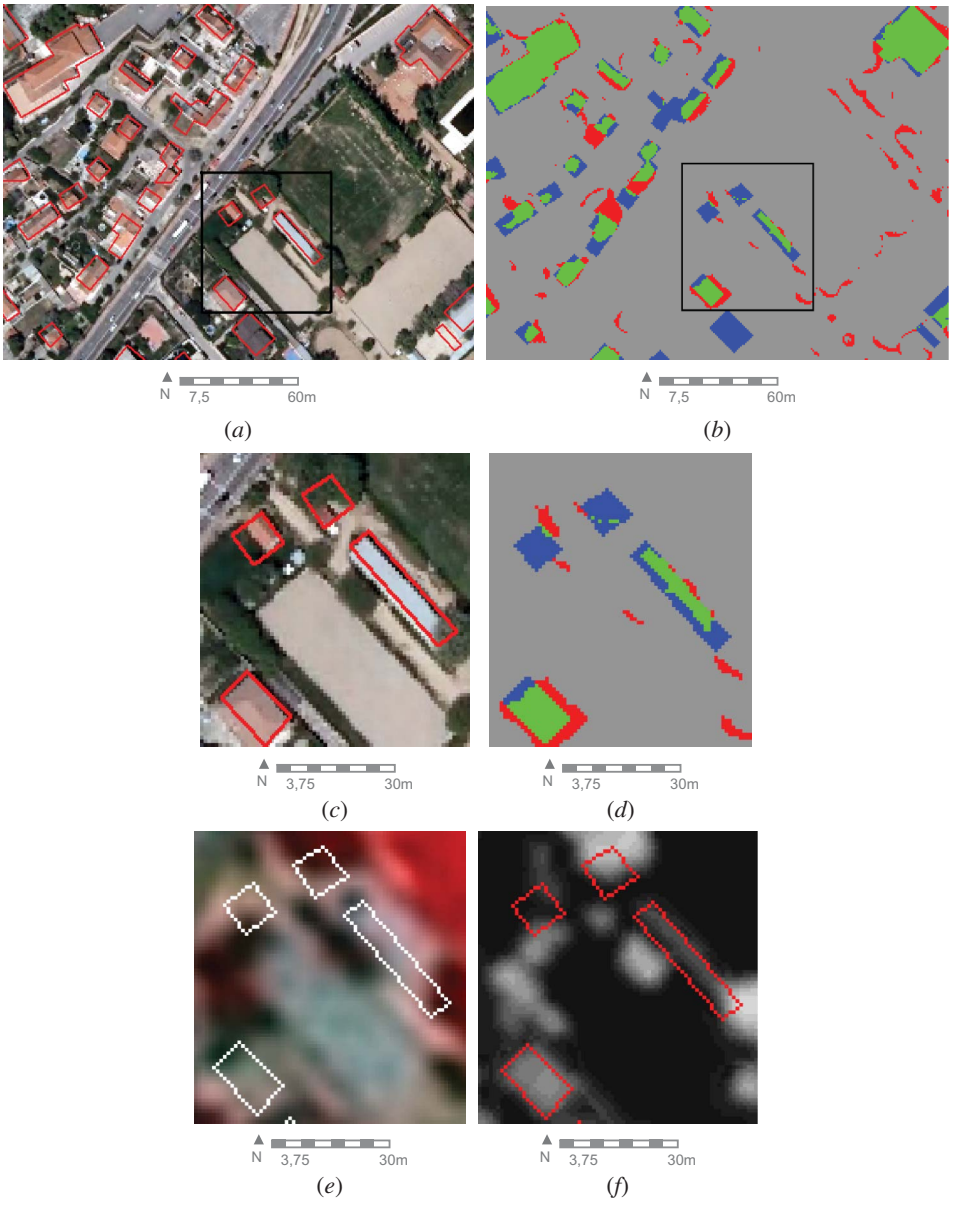

Figure 12. Detection of small buildings. (*a*) Aerial image of a residential area with vector cartography overlay; (*b*) results alter the application of the detection algorithm; (*c*) detail of (*a*) with aerial image and vectors; (*d*) results alter the application of the algorithm to (*c*); (*e*) pan-sharpened SPOT5 false colour image for the detail shown in (*c*); and (*f*) DSM obtained from the lidar data for (*c*).

experiments, we had no means to tune the parameters to obtain a clear separation of the two classes: vegetation and buildings. We blame this lack of infrared information on the aerial imagery. The need for infrared information has also been reported by Hermosilla, Ruiz, and Recio (2010). Calculation of a proper vegetation index such as NDVI is not possible

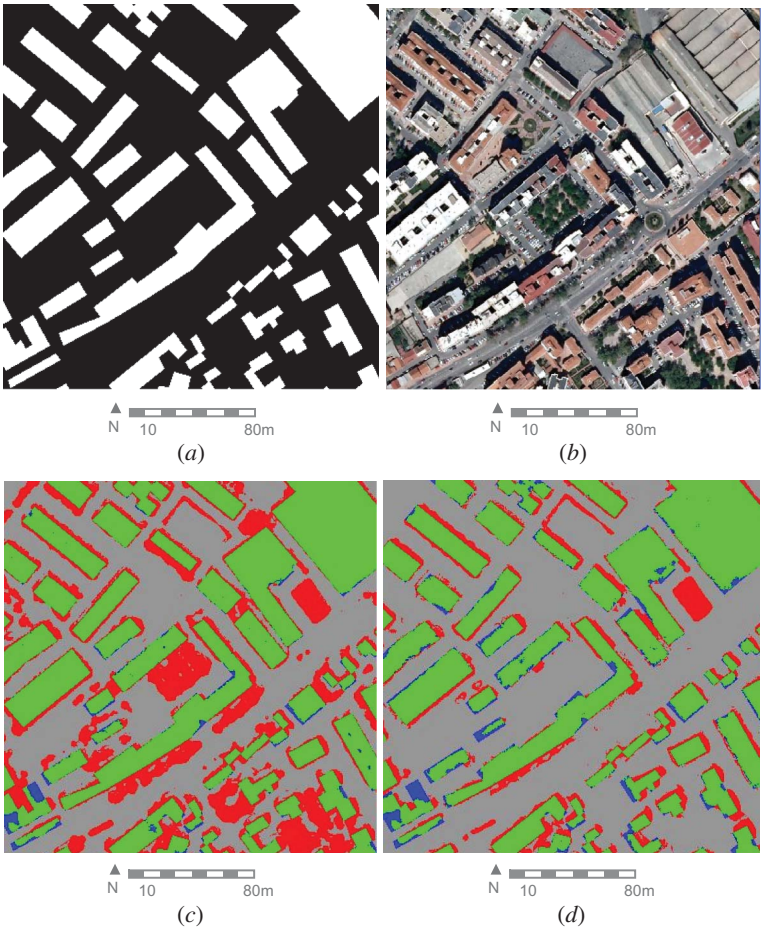

Figure 13. (*a*) Building mask; (*b*) aerial image; (*c*) result of the proposed algorithm with the aerial entry; and (*d*) result of the proposed algorithm with the SPOT5 entry.

without the infrared band; however, with the SPOT5 input, the separation between buildings and vegetation is quite good.

The aerial image in Figure 14(*a*) represents a new residential area of Alcalá. It shows that only four buildings in the vector cartography are represented; the rest of the buildings were constructed after the creation of the cartography. The proposed method has successfully detected all of these buildings except one (Figure 14(*b*)) with a purple-coloured tile roof (Figure 14(*c*)). This is a unique, large-sized building (about 1000 m^2) that is not detected by the proposed algorithm. As such, it is considered to be a false negative. This building appears as purple, a colour that is not seen in other tile roofs. Hence, the building must be made of a material with a very different spectral signature from all of the other buildings in the entire image.

Another error, a false positive, corresponds to the bridges on the highways. In Figure 15(*c*), these bridges were detected as buildings because, in the DSM, the bridges are seen to have height.

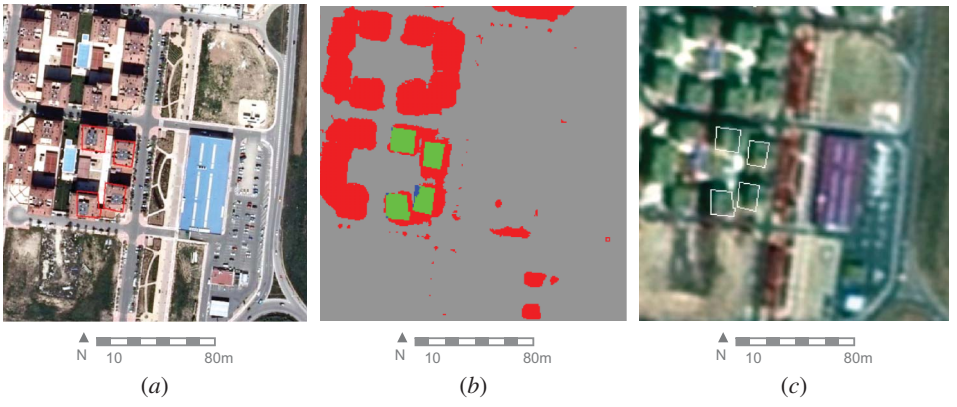

Figure 14. Detection of new buildings. (*a*) Aerial image; (*b*) results from the algorithm; and (*c*) SPOT5 image in false colour of (*a*).

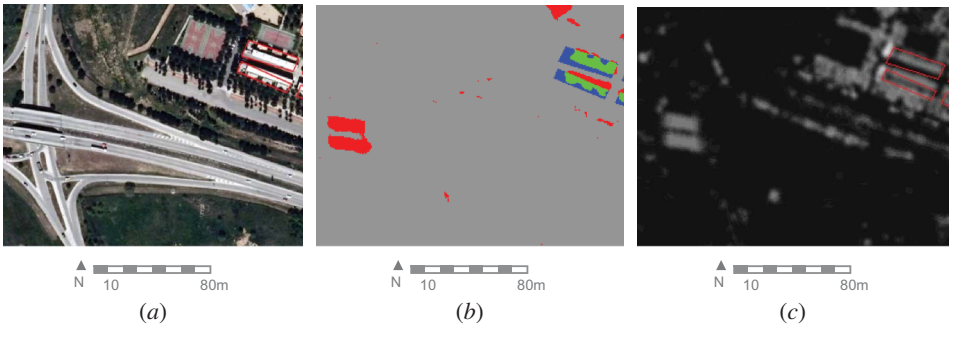

Figure 15. Detection of bridges as buildings. (*a*) Aerial image; (*b*) algorithm result; and (*c*) DSM corresponding to image (*a*).

5.3. Evaluation

Validation can be achieved by studying the buildings or the pixels that have changed. In this study, we investigated validation with regard to the buildings. A vector map that represents the true terrain has been manually constructed for a part of the entire image. This vector map corresponds to the upper right area of the initial image and is part of the university campus and its surroundings, a semi-urban zone of the city of Alcalá with a size of 4 km^2 (2 km $\times$ 2 km). This area contains approximately 200 buildings of different sizes, as shown in Figure 16.

In addition to the visual evaluation, a numerical evaluation would be of interest. Therefore, the validation of the formulae indicated in Heipke et al. (1997) and Rottensteiner et al. (2005) is also used:

$$\text{completeness} = \frac{\text{TP}}{\text{TP} + \text{FN}} \in [0, 1], \tag{1}$$

$$\text{correctness} = \frac{\text{TP}}{\text{TP} + \text{FP}} \in [0, 1]. \tag{2}$$

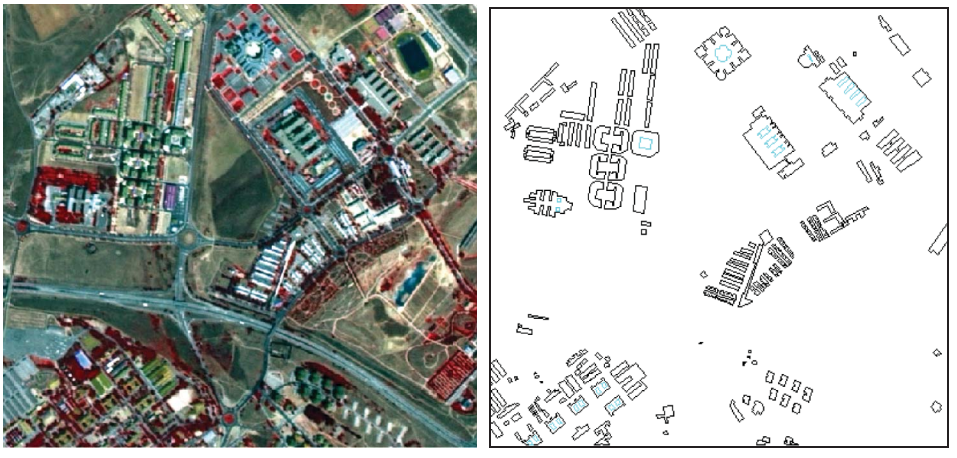

Figure 16. SPOT5 image and ground truth (manually constructed).

Here, TP is the number of true positives, which represent the new buildings that have been detected correctly; FN is the number of false negatives, which represent the buildings that the proposed method detects as unchanged, but that nevertheless have changed; and FP is the number of false positives, which represent the buildings that the proposed method detects as changed but are actually unchanged. Finally, TN, the true negative, indicates the buildings detected as not changed, which indeed have not changed; these appear in green.

Completeness and correctness are two measures that quantify the effectiveness of the method used to detect the changes from a practical point of view. The first measurement could be said to address the errors that remain in the final database once it has been updated, whereas the second measurement is related to the time necessary for a human operator to verify that the buildings have not changed.

For the validation of the method, only buildings with a ground surface greater than 25 m^2 were selected. The noise of the proposed method was not considered. In fact, if we view the purpose of the algorithm as being to aid human operators in updating the cartographic information, then when the operators see very small red or green spots, they are unlikely to pay any attention to them. The operators would consider the changes in buildings to be of little or no interest, since they will be looking for bigger changes.

With regard to new constructions, we could say that the detection of the algorithm is very satisfactory, since it detects 98% (46/47) (see Table 1). The only failure is in the detection of the building with the blue roof in Figure 10(*a*) or the building with the purple

Table 1. Confusion matrix for detected changes against actual changes, for buildings with ground surface greater than 25 m^2.

		Detected by the algorithm	
		Change	No change
Actual	Change	TP = 46	FN = 1
	No change	FP = 0	TN = 135

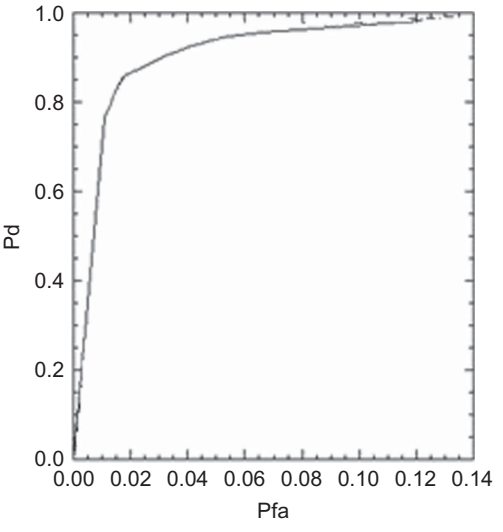

Figure 17. ROC curve that provides the probability of a false alarm (Pfa) versus the probability of detection (Pd) curve.

roof in Figure 14(*c*). As noted above, these detections could be the result of the strange materials used in the construction of these tile roofs. As seen in Equations (1) and (2) and Table 1, a completeness of 0.98 and a correctness of 1 are obtained for buildings with ground surface greater than 25 m^2.

With regard to the total number of buildings (including ground surface smaller than 25 m^2) on the validation image, the method detects 93% (181/194). Almost all of the undetected buildings corresponded to small houses or huts that appeared in the BCN but were too small to be detected with the input data (see Figure 12).

When the entire image is considered, the bridges and the hill are false positives, as mentioned above. The area of the image is very well known to some of the authors, and the algorithm has detected most of the changes. Although a human operator will have to perform a final manual edit to correct some errors, these changes will be minimal.

The receiver operating characteristic (ROC) method, applied to medical images for the evaluation of classifiers (Swets 1979), draws the detection probability against the false alarm probability. As explained in Section 4.2.2, the SVM was trained for the zone illustrated in Figure 16. It was later validated with the sample (1 km × 1 km) of the true terrain collected manually. Twenty thresholds were used to construct the ROC curve for the proposed algorithm. The result is shown in Figure 17.

The accuracy of a classifier can be measured by the area under the ROC curve (Hanley 1982; Fawcett 2006). An area of 1 represents a perfect classifier. An area of 0.5 represents a poor classifier. The following is a rough guide for the accuracy of a classifier: 0.5–0.6: fail; 0.6–0.7: poor; 0.7–0.8: fair; 0.8–0.9: good; and 0.9–1: excellent. In this study, the area under the curve was 0.95 for the proposed algorithm.

6. Conclusions

A method has been presented that allows the detection of changes between digital cartography, satellite images, and lidar data that occur between two specific dates. The developed computer application is a tool that can help a human operator in the cartographic

updating of 1:25,000 scale topographic maps. The method uses the traffic-light technique to detect new buildings and those that have disappeared, with 98% accuracy.

The proposed method allows discrimination of which buildings (or parts of buildings) have changed. Since the resolution of the SPOT5 images is 2.5 m, it can detect changes in only those buildings that have a ground plant size greater than 2.5 m × 2.5 m, i.e. greater than a pixel. Superior results are obtained with SPOT5, rather than PNOA, aerial images, although the latter provide greater spatial resolution and a superior radiometric quality. The reason for this is that the aerial image captures only RGB bands, whereas the SPOT5 images allow for two infrared bands, which provide a greater capacity to discriminate objects, especially vegetation. In future flights, the Spanish NMA plans to capture lidar data and simultaneously obtain aerial images in RGB plus near infrared. In that case, with small modifications, the method developed in this study would be applicable to these new data. The results would be expected to improve an operator's ability to detect smaller buildings that cannot now be detected with SPOT5.

The novelty of this method, when compared to other methods presented in the literature, is the use of SVM and the automatic training from the vectorial database. This provides operators with a fast semi-automatic approach for detecting buildings using satellite imagery and laser scanner data. Although we have used the protocol established by EuroSDR for comparison between algorithms, it is difficult to compare this study's proposed method with the other methods in the literature (Champion et al. 2009a) because all current methods are semi-automatic methods and each one uses a different set of input data, different types of classification algorithms, and different amounts of manual work. What can be said of our proposed method is that it is effective due to the high degree of accuracy obtained. Consequently, the intervention of an operator to edit the errors will be minimal.

With the tiling technique of the implementation, our proposed method will run for any data size. Consequently, the method would be completely operational in an industrial environment.

References

Alonso, M. C., and J. A. Malpica. 2008. "Classification of Multispectral High-Resolution Satellite Imagery Using LiDAR Elevation Data." *Lecture Notes in Computer Science* 5359: 85–94.

Arozarena, A., and G. Villa. 2005. "Plan Nacional De Ortofotografía Aérea De España (PNOA)." *(Spanish National Plan of Aerial Orthophotos) Topografía Y Cartografía: Revista Del Ilustre Colegio Oficial De Ingenieros Técnicos En Topografía* 22: 30–41.

Boser, B. E., I. Guyon, and V. N. Vapnik. 1992. "A Training Algorithm for Optimal Margin Classifiers." In *Proceedings of the Fifth Annual Workshop on Computational Learning Theory 5*, Pittsburgh, 144–52. San Mateo, CA: ACM Press.

Champion, N., F. Rottensteiner, L. Matikainen, X. Liang, J. Hyyppä, and B. P. Olsen. 2009a. "A Test of Automatic Building Change Detection Approaches." In *CMRT09*, IAPRS, Vol. XXXVIII, Part 3/W4, September 3–4, 2009, Paris, 145–50.

Champion, N., G. Stamon, and M. Pierrot-Deseilligny. 2009b. "Automatic GIS Updating from High Resolution Satellite Images." In *IAPR Machine Vision Applications*, May 20–22, Yokohama, Japan, 12-1: 374–7.

Chen, Y., W. Su, J. Li, and Z. Sun. 2009. "Hierarchical Object Oriented Classification Using Very High Resolution Imagery and LIDAR Data Over Urban Areas." *Advances in Space Research* 43: 1101–10.

Coppin, P., I. Jonckheere, K. Nackaerts, and B. Muys. 2004. "Digital Change Detection Methods in Ecosystem Monitoring: A Review." *International Journal of Remote Sensing* 25: 1565–96.

Fawcett, T. 2006. "An Introduction to ROC Analysis." *Pattern Recognition Letters* 27: 861–74.

Hanley, J. A. 1982. "The Meaning and Use of the Area under a Receiver Operating Characteristic (ROC) Curve." *Radiology* 143: 29–36.

Hao, Z. F., B. Liu, and X. W. Yang. 2006. "A Comparison of Multiclass Support Vector Machine Algorithms." In *Proceedings of the Fifth International Conference on Machine Learning and Cybernetics*, August 13–16, Dalian (IEEE), China, 4221–6.

Hayes, D. J., and A. Sader. 2001. "Comparison of Change Detection Techniques for Monitoring Tropical Forest Clearing and Vegetation Regrowth in a Time Series." *Photogrammetric Engineering and Remote Sensing* 67: 1067–75.

Heipke, C., H. Mayer, C. Wiedemann, and O. Jamet. 1997. "Evaluation of Automatic Road Extraction." In *IAPRS*, XXXII 3-4W2, July 1–7, Stuttgart, Germany, 151–60.

Hermosilla, T., L. A. Ruiz, and J. A. Recio. 2010. "Detección Automática de Edificios Mediante Imágenes de Alta Resolución y Datos LiDAR Para La Actualización de Bases de Datos Cartográficas En Entornos Urbanos." *Revista de Teledetección* 34: 89–93.

Huang, C. Y., and L. C. Chen. 2007. "Detection of Building Changes from LiDAR Data and Aerial Imagery." In *Proceedings of the 28th Asian Conference on Remote Sensing* (ACRS'07), November 12–16, Kuala Lumpur, Malaysia (on CD-ROM).

Knudsen, T., and A. A. Nielsen. 2004. "Detection of Buildings through Multivariate Analysis of Spectral, Textural, and Shape Based Features." In *Proceedings of the IEEE International Geosciences and Remote Sensing Symposium (IGARSS)*, September 20–24, Anchorage, Alaska, 2830–3.

Kraak, M. J., and F. Ormeling. 2003. *Cartography: Visualization of Geospatial Data*. 2nd ed. London: Pearson Education.

Lhomme, S., D. C. He, C. Weber, and D. Morin. 2009. "New Approach to Building Identification from Very-High-Spatial Resolution Images." *International Journal of Remote Sensing* 30: 1341–54.

Liu, Z., P. Gong, P. Shi, H. Chen, L. Zhu, and T. Sasagawa. 2010. "Automated Building Change Detection Using UltraCamD Images and Existing CAD Data." *International Journal of Remote Sensing* 31: 1505–17.

Lu, D., P. Mausel, E. Brondizio, and E. Moran. 2003. "Change Detection Techniques." *International Journal of Remote Sensing* 25: 2365–407.

Malpica, J. A., J. B. Mena, and F. J. Gonzalez-Matesanz. 2007. "Extraction of Cartographic Features from a High Resolution Satellite Image." In *Advances in Visual Computing ISVC07*. *Part II LNCS 4842*, edited by G. Bebis, R. Boyle, B. Parvin, D. Koracin, N. Paragios, S.-M. Tanveer, T. Ju, Z. Liu, S. Coquillart, C. Cruz-Neira, T. Muller, and T. Malzbender, 611–20. Berlin: Springer-Verlag.

Mancini, A., E. Frontoni, and P. Zingaretti. 2010. "Road Change Detection from Multi-Spectral Aerial Data." *International Conference on Pattern Recognition*, August 23–26, Istanbul, Turkey, 448–51.

Marcal, A. R. S., J. S. Borges, J. A. Gomes, and J. F. Pinto Da Costa. 2005. "Land Cover Update by Supervised Classification of Segmented ASTER Images." *International Journal of Remote Sensing* 26: 1347–62.

Martinez De Agirre, A., and J. A. Malpica. 2010. "Constructing a Digital Terrain Model from LiDAR Data." Chap. 4 in *Advances in Geoinformation Technologies*, edited by Jiri Horak, Lena Halounova, Tomas Hlasny, Dagmar Kusendova, and Vit Vozenilek, 47–59. Czech Republic: Institute of Geoinformatics.

Matikainen, L., J. Hyyppä, and H. Hyyppä. 2003. "Automatic Detection of Buildings from Laser Scanner Data for Map Updating." In *IAPRS*, XXXIV-3/W13, October 8–10, Dresden, Germany, 218–24.

Matikainen, L., J. Hyyppä, and H. Kaartinen. 2004. "Automatic Detection of Changes from Laser Scanner and Aerial Image Data for Updating Building Maps." In *IAPRS*, XXXV-B2, July 12–23, Istanbul, Turkey, 434–9.

Matikainen, L., K. Kaartinen, and J. Hyyppä. 2007. "Classification Tree Based Building Detection from Laser Scanner and Aerial Image Data." In *IAPRS*, XXXVI-3/W52, Espoo, Finland, 280–6.

Mayunga, S. D., D. J. Coleman, and Y. Zhang. 2007. "A Semi-Automated Approach for Extracting Buildings from QuickBird Imagery Applied to Informal Settlement Mapping." *International Journal of Remote Sensing* 28: 2343–57.

Mena, J. B., and J. A. Malpica. 2005. "An Automatic Method for Road Extraction in Rural and Semi-Urban Areas Starting from High Resolution Satellite Imagery." *Pattern Recognition Letters* 26: 1201–20.

Nakagawa, M., and R. Shibasaki. 2008. "Building Change Detection Using 3-D Texture Model." In *IAPRS*, XXXVII-B3a, July 3–11, Beijing, China, 173–8.

Niederöst, M. 2003. "Detection and Reconstruction of Buildings for Automated Map Updating." PhD thesis, ETH Zurich, Institut fur Geodasie and Phtotgrammetrie, Eidgenäossische Technische Hochschule.

Olsen, B. P. 2004. "Automatic Change Detection for Validation of Digital Map Databases." In *IAPRS*, XXXV-B3, July 12–23, Istanbul, Turkey, 120–5.

Olsen, B. P., and T. Knudsen. 2005. "Automated Change Detection for Validation and Update of Geodata." In *Proceedings of the 6th Geomatic Week*, February 8–11, Barcelona, Spain (on CD-ROM).

Olsen, B. P., and T. Knudsen. 2006. *Building Change Detection: A Case Study Comparing Results from Analog and Digital Imagery*. Technical report, KMS (National Survey and Cadastre) and Danish National Space Centre.

Peng, J., and Y. C. Liu. 2005. "Model and Context-Driven Building Extraction in Dense Urban Aerial Images." *International Journal of Remote Sensing* 26: 1289–307.

Raber, G. T., J. R. Jensen, S. R. Schill, and K. Schuckman. 2002. "Creation of Digital Terrain Models Using an Adaptive LiDAR Vegetation Point Removal Process." *Photogrammetric Engineering and Remote Sensing* 68: 1307–15.

Rottensteiner, F., J. Trinder, S. Clode, and K. Kubik. 2005. "Using the Dempster–Shafer Method for the Fusion of LiDAR Data and Multi-Spectral Images for Building Detection." *Information Fusion* 6: 283–300.

Streutker, D. R., and N. F. Glenn. 2006. "LIDAR Measurement of Sagebrush Steppe Vegetation Heights." *Remote Sensing of Environment* 102: 135–45.

Swets, J. A. 1979. "ROC Analysis Applied to the Evaluation of Medical Imaging Techniques." *Investigative Radiology* 14: 109–21.

Toutin, T. 2004. "Geometric Processing of Remote Sensing Images: Models, Algorithms and Methods (Review Paper)." *International Journal of Remote Sensing* 10: 1893–924.

Vapnik, V. 1995. *The Nature of Statistical Learning Theory*. New York: Springer-Verlag.

Vosselman, G., B. G. H. Gorte, and G. Sithole. 2004. "Change Detection for Updating Medium Scale Maps Using Laser Altimetry." *IAPRS* 34: 207–12.

Wald, L. 2002. *Data Fusion: Definitions and Architectures Fusion of Images of Different Spatial Resolutions*. Paris: Les Presses, Ecole des Mines de Paris.

Wang, Z., D. Ziou, C. Armenakis, D. Li, and Q. Li. 2005. "A Comparative Analysis of Image Fusion Methods." *IEEE Transactions on Geoscience and Remote Sensing* 43: 1391–402.